Sugar Signaling Induces Dynamic Changes during Meristem Development in Arabidopsis

Magdalena Musialak-Lange[1], Katharina Fiddeke[1,†,#], Annika Franke[1,†,#], Friedrich Kragler[1], Christin Abel[1], and Vanessa Wahl[1,*]

Affiliations:

[1]Max Planck Institute of Molecular Plant Physiology, Department of Metabolic Networks, Am Mühlenberg 1, Potsdam, 14476, Germany.

[†]Current work addresses: ProBioGen AG, Herbert-Bayer-Str. 8, 13086 Berlin (K.F.) and Takeda GmbH, Lehnizstra. 70-98, 16515 Oranienburg (A.F.)

[#]K.F. and A.F. contributed equally

*Correspondence to: vanessa.wahl@mpimp-golm.mpg.de.

One Sentence Summary:

The increase in meristem size during the floral transition is regulated via a feedback regulation involving sugar signaling.

Aerial parts of plants originate from pluripotent cells in the shoot apical meristem (SAM). This population of stem cells is maintained via a negative feedback loop involving stable expression of *WUSCHEL* (*WUS*) and *CLAVATA3*. SAM size is dynamic and undergoes a more than 2-fold expansion upon the transition to reproductive growth. The underlying mechanism controlling this process is largely unknown, but coinciding increased levels of trehalose 6-phosphate (T6P) suggest a participation of sugar signaling. Here we show that *TREHALOSE PHOSPHATE PHOSPHATASE J*, a component of the T6P pathway, is directly regulated by WUS, and controls SAM expansion at floral transition through WUS. Our findings demonstrate a dynamic feedback-regulation between central meristem maintenance and flowering time regulators with sugar signaling.

25 During the floral transition the *Arabidopsis thaliana* SAM undergoes a dramatic increase
26 in size[1] (Fig. 1a). Since the transition between developmental stages requires a massive
27 reorganization of organ development and sufficient energy, it is tightly controlled by
28 environmental conditions and availability of nutrients[2-5]. Hence, plant development as a whole
29 and SAM maintenance in particular demands continuous cross talk between its regulatory
30 processes and the available resources. The sugar phosphate, trehalose 6-phosphate (T6P), serves
31 as a signal for sucrose availability, which is conveyed to downstream metabolic and growth
32 responses through a still largely unknown mechanism[6]. Also knowledge on the underlying
33 mechanism controlling the morphological processes at the SAM at floral transition is scarce.
34 However, increased levels of T6P coincide with the floral transition and the T6P pathway
35 induces flowering by regulating key flowering genes expressed in leaves and the SAM[4], which
36 suggests a participation of sugar signaling in regulating the SAM size changes throughout the
37 floral transition.

38 To assess whether the morphological changes at the SAM involve the T6P pathway, we
39 investigated the effect on SAM architecture by decreasing *TPS1*, coding for the T6P synthesizing
40 enzyme, by the means of an artificial microRNA also in the SAM proper (*35S:amiRTPS1,* Fig.
41 S1). We compared these lines with plants with increased *TPS1* in the central zone (*CLV3:TPS1*,
42 Fig. S2). These have smaller and bigger vegetative and reproductive meristems (Fig. 1b, 1c),
43 resulting in smaller and bigger plants, respectively[4]. The homeodomain transcription factor WUS
44 and the signaling peptide CLV3 non-cell autonomously contribute to communication of position-
45 dependent properties among SAM cells in a negative feedback loop and maintain the SAM cell
46 population[7]. We therefore analyzed their expression in the SAM with altered *TPS1*. While the
47 expression of *WUS* in the organizing centre (OC) and *CLV3* in the central zone (CZ) harboring

48 the stem cells are considered mutually exclusive[7], we found reduced *TPS1* levels
49 (*35S:amiRTPS1*) lead to an enlarged OC domain marked by *WUS* (Fig. 1d) that overlaps with the
50 CZ, marked by *CLV3* expression (Fig. 1D). Plants overexpressing *TPS1* (*35S:TPS1*, Fig. S2)
51 display an increased stem cell pool with otherwise little effect on *WUS* expression (Fig. 1d).
52 However, the size of the CZ decreases in plants expressing *TPS1* under the *CLV3* promoter (Fig.
53 1d, Fig. S2), indicating a smaller stem cell pool in support of a much smaller SAM size
54 phenotype (Fig. 1d) of the very early flowering *CLV3:TPS1* plants[4]. The expression of
55 *HISTONE4, CYCLIN D3;1* and *CYCLIN-DEPENDENT KINASE2;1*, three cell cycle marker
56 genes (Fig. S3), suggests a higher proliferation rate and an increased number of cells displaced
57 from the CZ to adopt organ-specific cell fates at the periphery as a plausible reason for the
58 decreased SAM size of *CLV3:TPS1* and *vice versa* increased SAM size of *35S:amiRTPS1* plants
59 (Fig. 1b, 1c).

60 To assess whether the WUS/CLV feedback loop can uncouple in a wild-type SAM
61 during normal growth, we analyzed *WUS* and *CLV3* expression in wild-type plants in a time
62 series spanning the floral transition (Fig. 1e). Throughout the vegetative phase SAM size
63 gradually increases due to rising cell numbers (Fig. 1a; Fig. S4)[8], reaching its maximum at the
64 floral transition, independent of whether the plants are grown in continuous long days (LD) (Fig.
65 1a) or in short days (SD) followed by a transfer to LD (Fig. S5). An enlarging SAM at the floral
66 transition correlates with a larger *WUS* expression domain expanding into the CZ and the outer
67 cell layer (L1) (Fig. 1e-g). This is supported by larger meristems of the *35S:amiRTPS1* line,
68 which express *WUS* in the central zone (Fig. 1d). This observation is also consistent with
69 massive proliferation of meristematic cells detected when *WUS* is expressed from a *CLV3*
70 promoter in the CZ that resulted in meristems, no longer producing organs[9]. The presence of

71 *WUS* transcript in the outer meristem layers might be explained by a transient cytokinin signal in
72 L1, which induces *WUS* and was reported to respond to carbon in seedlings[10-12]. However,
73 cytokinin levels seem not to be altered in the L1 layer of cells as indicated by the synthetic
74 cytokinin reporter *TCSn:GFP*[13] (Fig. S6). Further, while *WUS* expands to L1 for a short period
75 (8-10 DAG), the *CLV3* expression domain remains expanded post floral transition (Fig. 1e, 1h).
76 This suggests a transient uncoupling, which is re-established at the reproductive SAM (16 DAG),
77 resembling earlier vegetative SAM expression patterns (6 DAG) (Fig. 1e), allowing organ
78 production to resume.

79 To understand how the T6P pathway might control this process, we first analyzed
80 expression of the ten genes encoding TREHALOSE PHOSPHATE PHOSPHATASEs (TPP)[6].
81 Except for *TPPC* and *TPPD*, which are expressed below detection limit, all were expressed in
82 distinct SAM domains (Fig. S7). *TPPJ* strongly increases in the enlarged SAM of *clv3-7* due to
83 an ectopic expression in L1 and L2 (Fig. 2a-c, Fig. S8, S9). Notably, in *clv3-7* and *clv3-10*
84 mutants high levels of *WUS* in the outer SAM layers (Fig S9)[14] coincides with ectopic expression
85 of *TPPJ* (Fig. S9). To assess whether ectopic expression of *TPPJ* contributes to the enlarged
86 SAM of the *clv3* mutant, we next overexpressed *TPPJ* (*35S:TPPJ*, Fig. 2d). This results in
87 significantly enlarged SAMs (Fig. 2e), and importantly, expands the *WUS* expression domain
88 into L1 (Fig. 2f), consistent with our finding in wild-type plants at the floral transition (Fig. 1e).

89 Overlapping expression domains of ectopic *TPPJ* (Fig. 2b) and *WUS* in the *clv3* mutant
90 SAM implies a direct influence of WUS on *TPPJ* expression. This is supported by an *in silico*
91 analysis which predicts multiple, canonical WUS binding sites in the sequence upstream of the
92 *TPPJ* coding sequence ($TPPJ^{WUS}$, Fig. 3a)[10,15-17]. WUS is a bifunctional transcription factor,
93 which was found to both activate and repress gene expression[7]. To understand if WUS directly

94 controls *TPPJ*, we performed *in vivo* transactivation assays. These show that WUS activates
95 reporter gene expression when using a 2865 bp *TPPJ* 5' sequence, containing 17 putative
96 *TPPJ*^{WUS} sites (Fig. 3a). Progressive deletion of the *TPPJ* 5' sequence results in a reduction of
97 reporter gene activation, suggesting an additive effect of the individual *TPPJ*^{WUS} sites (#1-6; Fig.
98 3a, 3b). We confirmed the direct binding of WUS to three distinct regions of the *TPPJ* promoter
99 (I, II, and III, Fig. 3c-e, Fig. S10) by Chromatin immunoprecipitation (ChIP) coupled to PCR
100 using a specific antibody against WUS (Fig. S11), while all other regions did not indicate
101 binding (Fig. S10, Fig. S12). We observed enrichment of WUS binding to *TPPJ*^{WUS} elements up
102 to 0.67% of the input DNA in *clv3-7* and up to 0.75% of the input DNA in *clv3-10* apices, both
103 of which express *WUS* at high levels in comparison to input DNA from wild-type apices, where
104 *WUS* is expressed in only a few cells and input DNA from leaves, with no WUS (Fig. 3c-e; Fig.
105 S10). Lastly, electrophoretic mobility shift assays (EMSA) confirm *in vitro* binding of WUS to
106 the investigated sequences (I, II 1-3, III 1-3; Fig. 3f). In summary, we demonstrate that seven out
107 of 17 putative *TPPJ*^{WUS} sites are directly targeted by WUS *in vivo*.

108 To further assess the role of *TPPJ* at the SAM we used an artificial miRNA (*amiRTPPJ*)
109 approach to downregulate *TPPJ* (*35S:amiRTPPJ*) (Fig. S13). Similar to a *tppj* T-DNA insertion
110 mutant, plants overexpressing either of two versions of an *amiRTPPJ* (V1, V2) flower
111 significantly earlier in both LD and SD (*35S:amiRTPPJ*, Fig. S14, Table S1). *ML1* expression
112 specifically and stably localizes to the epidermis (L1) throughout the investigated developmental
113 stages (Fig. S15). *ML1:amiRTPPJ* plants reduce *TPPJ* expression in L1 (arrowheads in Fig.
114 S16), have smaller SAMs and flower significantly earlier in LD and SD (Fig. 4a-c, Fig. S17,
115 S18, Table S1), while the level of *TPPJ* reduction is proportional to the acceleration of flowering
116 (Fig. 4b and c, Fig. S13, Table S1). To date there are no reports that mutants in meristem

117 maintenance genes are affected in their flowering time. We found that plants mutant for *CLV3*
118 are late flowering (Fig. 4c, Table S1). However, when *ML1:amiRTPPJ* is introgressed into either
119 the *clv3-7* or *clv3-10* background, the late flowering phenotype of the mutant plants is restored to
120 wild type (Fig. 4c, Fig. S18, Table S1), suggesting that *TPPJ* expression in the epidermis is also
121 necessary for the late flowering phenotype of *clv3*. Hence, the early flowering of
122 *ML1:amiRTPPJ* in a wild-type background is due to a reduction of *TPPJ* expression in L1 in its
123 endogenous expression domain. In addition, other prominent morphological defects of *clv3-10*
124 such as fasciated stems and enormous inflorescence SAMs are visibly reduced in the presence of
125 *ML1:amiRTPPJ* (Fig. S18). *CLV3* expression increases to much higher levels in *ML1:amiRTPPJ*
126 than in plants overexpressing *TPPJ* (Fig. 4d), suggesting an active role of the T6P pathway in the
127 outer SAM layer with regard to stem cell maintenance. In addition, *WUS* is induced (Fig. 4d, Fig.
128 S19), indicating uncoupling of the WUS/CLV feedback loop, consistent with our findings with
129 altered T6P signaling at the SAM (Fig. 1d, Fig. 2f).

130 Since the T6P pathway influences the age pathway at the SAM [4], we analyzed mature
131 miR156 as well as the expression of *SPL3*, *SPL4*, *SPL5*, *SPL9* and *SPL15*, all associated with
132 floral transition in general[18,19] (Fig. S20, Table S1). We found a strong reduction of mature
133 miR156 levels correlating with lower *TPPJ* expression in *ML1:amiRTPPJ*, and corresponding
134 increased expression of *SPL3, SPL4, SPL5*, and *SPL9* (Fig. 4e). In line, miR156 abundance was
135 highly increased in *TPPJ* overexpressing plants, while the corresponding *SPL*s were
136 downregulated (Fig. 4e). However, expression of *SPL15*, previously described to be mainly
137 responsible for integrating the aging stimulus into the regulation of the floral onset[20], was not
138 differentially expressed in either of the transgenic lines (Fig. S21). In addition, we found miR156
139 levels significantly increased in *clv3-10* mutant apices (Fig. 4f). In response, the levels of *SPL3*,

140 *SPL5*, and *SPL9* were reduced in line with the late flowering phenotype of the mutant. In contrast
141 to what would be expected, we found more *SPL4* in apices of the late flowering *clv3-10* (Fig. 4f).
142 Higher order lines from *spl3*, *spl4* and *spl5* deletion mutant plants are significantly later
143 flowering in all lines with *spl4* (Fig. S20, Table S1). This argues for an important role of *SPL4* in
144 inducing flowering. *SPL4*, similar to *SPL3*, *SPL5* and *SPL9,* is induced at the wild-type SAM at
145 floral transition[21]. However, it is expressed in the very center of the SAM, in a domain largely
146 overlapping with the WUS protein domain[5,17,20,22], while *SPL3*, *SPL5*, and *SPL9* are expressed at
147 the periphery of the SAM and in the vasculature of young leaves[5,20]. This might denote a direct
148 regulation of *SPL4* by WUS, which would explain increased *SPL4* in the *clv3* mutant
149 background (Fig. 4f) and the previously identified partially miR156-dependent regulation of the
150 *SPL*s by the T6P pathway[4]. Indeed, we identified a larger number of potential *SPL4*^{WUS} sites
151 upstream of the *SPL4* coding sequence when compared to the 5' intergenic regions of the other
152 *SPL*s (Fig. S22). However, this finding also suggests that additional players downstream of
153 CLV3 are important for the onset of flowering, which cannot be bypassed by an otherwise
154 inductive SPL4 (Fig. 4f). Since carbohydrate status regulates timing of the floral transition[4], it is
155 interesting that T6P signaling also directly influences the re-organisation of the SAM during the
156 floral transition (Fig. 4g). Given the ubiquitous nature of carbohydrate signaling and the large-
157 scale change in sink-source relationships within the plants[23], it will be interesting to determine if
158 this regulatory mechanism is widely present in the plant kingdom.
159

160 **Methods**

161 **Materials and Methods**

162 Plant material and growth conditions

163 All *Arabidopsis thaliana* plants used for this study are of the Columbia accession (Col-0).
164 The lines *clv3-7*[24], *clv3-10*[25], *35S:amiRTPS1*, *CLV3:TPS1*[4], and *WUS:WUS:GFP*[22] have been
165 described previously as indicated. Plants were grown in controlled growth chambers at 22°C in
166 long day (LD, 16h light/8h dark) or short day (SD, 8h dark/16h light) conditions with a light
167 intensity of approximately 160 µmol/m^{-2}s^{-1} and a relative humidity of 60-65%. Controlled
168 induction of flowering was performed using a previously described shift protocol[21].

169 Phenotypic analysis

170 Flowering time was defined as days to flowering (DTF), recorded when shoots were 0.5 cm
171 high (bolting), and by scoring the total leaf number (TLN). The TLN is the sum of rosette leaves
172 (RLN, rosette leaf number) and cauline leaves (CLN, cauline leaf number) per plant (Table S1).
173 On average 20 plants of each genotype were analyzed in one experiment. Plants were grown in
174 the conditions described above, and randomized every second day to avoid position effects.

175 Generation of transgenic lines

176 Generally, Col-0 plants were transformed by the floral dip method[26]. The presence of the
177 transgene was confirmed by PCR and independent, single-insertion, homozygous T3 plants
178 were selected and used for all further studies. Oligonucleotides used for cloning are provided in
179 Table S2, those used for genotyping are given in Table S3. To generate the *35S:TPPJ* and

180 *35S:TPS1* lines, the coding sequences of *TPPJ* (At5g65140) and *TPS1* (At1g78580) were amplified
181 and introduced into the *pGEM®-Teasy* vector (Promega, Madison, Wisconsin, US), sub-cloned
182 into the Gateway® entry vector pJLBlue reverse[27] (pVW275 and pVW099), and recombined into
183 a pGREEN-II-based destination vector with 35S promoter (pVW279 – *TPPJ* and pVW161 – *TPS1*)
184 using the Gateway® LR clonase II Enzyme mix (Invitrogen, Carlsbad, CA). Generation of artificial
185 microRNAs targeting *TPPJ* (*ML1:amiRTPPJ* V1 and V2, *35S:amiRTPPJ* V1 and V2) was performed
186 according to a previously published protocol[28] using the WMD3–Web MicroRNA Designer
187 (http://wmd3.weigelworld.org/cgi-bin/webapp.cgi). The resulting *Eco*RI/*Bam*HI fragment was
188 sub-cloned into the Gateway® entry vector *pJLBlue* reverse[27] (V1: pVW498, V2: pVW499) and
189 recombined using the Gateway® LR clonase II Enzyme mix (Invitrogen, Carlsbad, CA) into a
190 *pGREEN-II*-based destination vector with either the *ML1* or *35S* promoter (V1: pVW507, V2:
191 pVW508, V1: pVW504 V2: pVW505). Double mutant lines of *clv3* and *ML1:amiRTPPJ #1 and #2*
192 were generated through crosses. All lines were propagated to the F4 generation and tested for
193 homozygosity. To generate the *spl3, spl4, spl5,* knockout lines a modified version of the two
194 single guided RNAs (2sgRNA) CRISPR/*Cas9* technology was used[29,30]. In brief, the NGG PAM
195 recognition sites in the *5'UTR* and last exon of *SPL3*, first exon and *3'UTR* of *SPL4* and *5'UTR* and
196 *3'UTR* of *SPL5* were defined using the ATUM webtool (https://www.atum.bio). *pJF1033* vector,
197 containing 2sgRNA scaffold, was used as a template. Resulting *Bsa*I products were restriction
198 cloned into the *pJF1031* binary vector[30]. Plants with homozygous deletions for *SPL3, SPL4* or
199 *SPL5* were back-crossed to Col-0. Homozygous, *Cas9*-free lines were used for the experiments
200 and to generate all higher order mutations, i.e. the *spl34, spl35, spl45* double as well as the
201 *spl345* triple mutant lines.

202 RNA extraction and cDNA synthesis

203 Total RNA form homogenized rosette or dissected SAM samples was isolated by a
204 phenol/chloroform extraction method using a modified TRIzol reagent with the following
205 composition: phenol 38% (v/v), guanidine thiocyanate 0.8 M ammonium thiocyanate 0.4 M,
206 sodium acetate 0.1 M pH 5.0, glycerol 5% (v/v), EDTA 5 mM pH 8.0, Na-lauroylsarcosine 0.5%
207 (v/v). This was then followed by a sodium acetate precipitation to improve RNA purity. cDNA
208 synthesis, preceded with removal of putative genomic DNA contamination with Dnase I Rnase-
209 free (Ambion™/Thermo Fisher Scientific, Waltham, Massachusetts, US), was carried out using a
210 SuperScript™IV Reverse Transcriptase Kit (Thermo Fisher Scientific, Waltham, Massachusetts,
211 US) according to the manufacturer's instruction. For quantification of mature miR156 the
212 respective stem-loop primers (Table S4) were added to the cDNA synthesis reaction (1:1 with
213 oligo dT(18) primer) (Thermo Fisher Scientific, Waltham, Massachusetts, US) as previously
214 described[31].

215 RT-qPCR analysis

216 RT-qPCR analyses were performed with the ABI Prism 7900 HT fast real time PCR system
217 (Applied Biosystems/Life Technologies, Darmstadt, Germany) using a Power SYBR® Green-PCR
218 Master Mix (Applied Biosystems/Life Technologies, Darmstadt, Germany) in a 10 μl reaction
219 volume for expression analyses and in a 5 μl volume for ChIP-PCRs. All oligos are listed in Table
220 S4 and Table S5 (RT-qPCR and ChIP-PCR respectively). All data were analyzed using the SDS 2.4
221 software (Applied Biosystems/Life Technologies, Darmstadt, Germany) applying the criteria
222 described by Czechowski and co-workers (2004). cDNA quality was determined with primers

223 binding to the 3´ and 5´ regions of *GLYCERALDEHYDE-3-PHOSPHATE DEHYDROGENASE* (*GAPDH*,
224 At1g13440), and samples with Ct *5´GAPDH*/Ct *3´GAPDH* values > 1 were excluded from further
225 analyses. Expression values were calculated by the comparative Ct method using the reference
226 gene index (RGI) as previously described[4] and *POLYUBIQUITIN10* (*UBQ10*, At4g05320) for figure
227 3C and S14[32]. The primer sequences for the reference and analyzed genes are given in the Table
228 S4.

229 RNA *in situ* hybridization

230 Wax embedding was performed using an automated processor and embedding system
231 (Leica EG1160, Solms, Germany). Sections of 8 µm thickness were prepared using a rotary
232 microtome (Leica RM2265; Leica, Wetzlar, Germany).

233 Probes for RNA *in situ* hybridization were synthesized using the DIG RNA Labeling Kit
234 (Roche, Mannheim, Germany). For this the ORFs of the target genes were cloned into the
235 pGEM®-T Easy vector (Promega, Madison, Wisconsin, US) as a template according to
236 manufactures instructions (oligonucleotides and construct IDs listed in the Table S6) and the
237 sense and antisense RNA probes were synthetized using T7 and SP6 polymerases, respectively.
238 *RNA in situ* hybridizations were carried out as previously described[4]. The final sections were
239 imaged with an Olympus BX-61 microscope equipped with a DC View II digital camera (Olympus
240 Europa SE & Co, Hamburg, Germany).

241 Chromatin immunoprecipitation (ChIP)

242 For ChIP-PCR, 100 apices per biological replicate (Col-0, *clv3-7* and *clv3-10*) were collected
243 and snap frozen in liquid N_2. Samples were fixed in 1% (v/v) formaldehyde buffer (10 mM

244 sodium phosphate buffer, pH 7; 50 mM NaCl; 100 mM sucrose) under vacuum. ChIP was
245 performed as previously described[33] with modifications: Antibody incubation (anti-WUS; AS11
246 1759; Agrisera) was extended to o/n at 4°C and incubation with Agarose beads (Protein A-
247 Agarose; sc-2001; Santa Cruz Biotechnology) to 6 h at 4°C. Immunoprecipitated DNA was
248 analyzed by RT-qPCR assay. Data were analyzed using the SDS 2.4 software (Applied
249 Biosystems/Life Technologies, Darmstadt, Germany). Ct values of *TPPJ* promoter regions were
250 normalized to the Ct value of a region within the *UBQ10* promoter. The % of enrichment was
251 calculated as relative to the input expression of the individual *TPPJ* promoter regions. The
252 following controls were performed: ChIP on 100 apices of Col-0, *clv3-7* and *clv3-10* omitting
253 addition of AB and ChIP on 1.5 g of Col-0, *clv3-7* and *clv3-10* leaves (Fig. S. 10). Please note that
254 in contrast to the input samples there was no amplification in any of the other ChIP control
255 samples. Oligonucleotides are listed in the Table S5.

256 Transactivation assay

257 For the effector construct line, the *WUS* (At2g17950) coding sequence was PCR amplified
258 using the Phusion High-Fidelity DNA Polymerase (Thermo Fisher Scientific, Waltham,
259 Massachusetts, US). The resulting fragment was cloned into the pGEM®-Teasy vector (Promega,
260 Madison, Wisconsin, US) (pVW310), sub-cloned into the Gateway® entry vector pJLBlue
261 reverse[27] (pMML056) and recombined using the Gateway® LR clonase II Enzyme mix
262 (Invitrogen, Carlsbad, CA) into a Gateway® destination vector with 35S promoter (pMDC32)
263 (pMML058). For the reporter gene constructs, designated regions of the 5' TPPJ region were
264 amplified with specific primers (Table S2) using the Phusion High-Fidelity DNA Polymerase
265 (Thermo Fisher Scientific, Waltham, Massachusetts, US). The resulting *Kpn*I/*Acy*I fragment was

266 sub-cloned into the Gateway® entry vector pMDC162 to obtain GUS gene fusions (Table S2).
267 The 35Somega:LUC-NOS plasmid containing the LUC gene driven by the 35S promoter was used
268 as an internal control. Col-0 protoplasts were isolated from leaves of 4-week-old plants and
269 transfected by a modified polyethylene glycol method[34]. The transfected cells were incubated
270 for 20 h at 22°C in the light (100 µmol/$m^{-2}s^{-1}$), harvested by centrifugation at 100 g for 2 min,
271 and then lysed[35]. Luciferase activity was measured with a luciferase assay kit (Promega,
272 Madison, Wisconsin, US) according to the manufacturer's instruction, and GUS activity was
273 determined according to a previously described protocol[35].

274 Electrophoretic mobility shift assay (EMSA)

275 *WUS* coding sequence without STOP codon was PCR amplified using the Phusion DNA
276 polymerase (New England Biolabs). The resulting fragment was sub-cloned into the Gateway®
277 entry vector pDONR207 (pMML059) and recombined into a Gateway® destination vector with
278 35S promoter (pDEST24) using the Gateway® LR clonase II Enzyme mix (Invitrogen, Carlsbad,
279 CA) resulting in pMML063. The plasmid was transformed into the *Escherichia coli* strain Rosetta
280 plysS and the protein production was induced with 1 mM isopropyl β-D-1-
281 thiogalactopyranoside at 30°C over-night. Bacterial cell lysis was performed by sonication (1x, 5
282 sec, 20% power, 4 cycles, Sonoplus Hd 2070 Sonicator, Badelin, Berlin, Germany) preceded by
283 incubation on ice for 20 min in the freshly prepared protein extraction buffer (20 mM Na-
284 phosphate buffer, pH 7.4; 0.5 M NaCl; 1 mM phenylmethylsulfonyl fluoride; 1 mM
285 Ethylenediaminetetraacetic acid; 1 tablet of cOmplete™ Protease Inhibitor Cocktail (Merck,
286 Darmstadt, Grmany) per 10 ml of the buffer). For the EMSA 2 µg of protein (crude extract,
287 determined by Pierce™ BCA Protein Assay Kit, Thermo Fisher Scientific, Waltham,

288 Massachusetts, US) was used. The EMSA was performed using 5'-IRDey-682-labeled, double-
289 stranded oligos of 50 bp spanning the putative WUS binding sites in the 5' regulatory region of
290 *TPPJ* (Table S7). Binding reactions were carried out using the Odyssey® EMSA Kit (LI-COR®)
291 according to the manufacturer's instruction with a competitor to probe ratio of 1:200. Results
292 were visualized using an Oddysey Infrafed Imaging System (Li-Cor, Lincoln, NE).

293 Confocal microscopy

294 Apices from developmental series of Col-0 TCSn:GFP cytokinin reporter line lines were
295 excised using a diamond knife leaving a stalk of stem tissue. This stalk was used to fix the
296 sample for imaging in a droplet of 0.1% agar covered with Perfluorodecalin (F2 Chmicals,
297 Lancashire, UK) on a glass slide. A Leica SP8 confocal laser scanning system equipped with a
298 M6000B-CS microscopy stage, an Argon laser (65 mV), and a 40x water immersion HCX APO
299 objective was used to image SAMs with following settings: Laser output power 20%; GFP
300 Excitation (green): wavelength 488 nm / emission detection channel 3: 495 - 520 nm, gain PMT
301 800 V; plastid auto-fluorescence (blue) emission detection channel 4: 700 - 800 nm, gain PMT
302 ~500 V; scan speed 600 Hz in xyz bi-directional scanning mode with a z-stack distance of
303 approx. 10 µm. Offset = 0; pixel dimension: 1024 × 1024. To visualize the differences in GFP
304 presence middle sections of representative SAMs were extracted from z-stacks using the Fiji
305 software package[36], version 2.0.0-rc-69/1.52 max-intensity Z-Projection function.

306 Statistical consideration

307 Statistical significance of flowering time and RT-qPCR data was analyzed both, by one-way
308 ANOVA (Analysis of Variance) with Tukey' Post Hoc HSD (Honestly Significant Difference) based

309 on Tukey-Kramer correction (P value <0.05) and two-tailed Student's *t*-test. Significance of the
310 data was marked with asterisks (*) based on the following criteria: P ≤ 0,05: *, P ≤ 0,01: **, P ≤
311 0,001: ***. The presented statistical data are based on: flowering time experiments – min. 20
312 plants of each genotype; SAM area measurements – longitudinal middle section through min. 7
313 individual SAMs; *WUS* and *CLV3* expression domain size and distance to the summit –
314 longitudinal middle section through min. 6 individual SAMs RT-qPCR – min. three biological
315 replicates; Transactivation assay – 6 biological replications; ChIP – 3 biological replications.

316 **Data availability**

317 All data supporting the findings of this study are available in the main text or the
318 Supplementary Information. All biological materials used in this study are available from the
319 corresponding author on reasonable request. Source data are provided with this paper.

320 **References and Notes**

321 1 Kwiatkowska, D. Flowering and apical meristem growth dynamics. *J Exp Bot* **59**,
322 187-201, doi:10.1093/jxb/erm290 (2008).
323 2 Srikanth, A. & Schmid, M. Regulation of flowering time: all roads lead to Rome.
324 *Cellular and molecular life sciences : CMLS* **68**, 2013-2037, doi:10.1007/s00018-011-
325 0673-y (2011).
326 3 Ponnu, J. *et al.* The Trehalose 6-Phosphate Pathway Impacts Vegetative Phase
327 Change in Arabidopsis thaliana. *Plant J*, doi:10.1111/tpj.14965 (2020).
328 4 Wahl, V. *et al.* Regulation of flowering by trehalose-6-phosphate signaling in
329 Arabidopsis thaliana. *Science (New York, N.Y.)* **339**, 704-707,
330 doi:10.1126/science.1230406 (2013).
331 5 Olas, J. J. *et al.* Nitrate acts at the Arabidopsis thaliana shoot apical meristem to
332 regulate flowering time. *New Phytol* **223**, 814-827, doi:10.1111/nph.15812 (2019).
333 6 Fichtner, F. & Lunn, J. E. The Role of Trehalose 6-Phosphate (Tre6P) in Plant
334 Metabolism and Development. *Annu Rev Plant Biol*, doi:10.1146/annurev-arplant-
335 050718-095929 (2021).

7 Pfeiffer, A., Wenzl, C. & Lohmann, J. U. Beyond flexibility: controlling stem cells in an ever changing environment. *Curr Opin Plant Biol* **35**, 117-123, doi:10.1016/j.pbi.2016.11.014 (2017).
8 Kinoshita, A. *et al.* Regulation of shoot meristem shape by photoperiodic signaling and phytohormones during floral induction of Arabidopsis. *Elife* **9**, doi:10.7554/eLife.60661 (2020).
9 Brand, U., Grunewald, M., Hobe, M. & Simon, R. Regulation of CLV3 expression by two homeobox genes in Arabidopsis. *Plant Physiol* **129**, 565-575, doi:10.1104/pp.001867 (2002).
10 Leibfried, A. *et al.* WUSCHEL controls meristem function by direct regulation of cytokinin-inducible response regulators. *Nature* **438**, 1172-1175, doi:10.1038/nature04270 (2005).
11 Snipes, S. A. *et al.* Cytokinin stabilizes WUSCHEL by acting on the protein domains required for nuclear enrichment and transcription. *PLoS Genet* **14**, e1007351, doi:10.1371/journal.pgen.1007351 (2018).
12 Pfeiffer, A. *et al.* Integration of light and metabolic signals for stem cell activation at the shoot apical meristem. *Elife* **5**, doi:10.7554/eLife.17023 (2016).
13 Zurcher, E. *et al.* A robust and sensitive synthetic sensor to monitor the transcriptional output of the cytokinin signaling network in planta. *Plant Physiol* **161**, 1066-1075, doi:10.1104/pp.112.211763 (2013).
14 Brand, U., Fletcher, J. C., Hobe, M., Meyerowitz, E. M. & Simon, R. Dependence of stem cell fate in Arabidopsis on a feedback loop regulated by CLV3 activity. *Science (New York, N.Y.)* **289**, 617-619, doi:10.1126/science.289.5479.617 (2000).
15 Lohmann, J. U. *et al.* A molecular link between stem cell regulation and floral patterning in Arabidopsis. *Cell* **105**, 793-803, doi:10.1016/s0092-8674(01)00384-1 (2001).
16 Sloan, J. *et al.* Structural basis for the complex DNA binding behavior of the plant stem cell regulator WUSCHEL. *Nat Commun* **11**, doi:ARTN 2223 10.1038/s41467-020-16024-y (2020).
17 Yadav, R. K. *et al.* WUSCHEL protein movement mediates stem cell homeostasis in the Arabidopsis shoot apex. *Genes Dev* **25**, 2025-2030, doi:10.1101/gad.17258511 (2011).
18 Hyun, Y., Richter, R. & Coupland, G. Competence to Flower: Age-Controlled Sensitivity to Environmental Cues. *Plant Physiol* **173**, 36-46, doi:10.1104/pp.16.01523 (2017).
19 Xie, Y. *et al.* FHY3 and FAR1 Integrate Light Signals with the miR156-SPL Module-Mediated Aging Pathway to Regulate Arabidopsis Flowering. *Mol Plant* **13**, 483-498, doi:10.1016/j.molp.2020.01.013 (2020).
20 Hyun, Y. *et al.* Multi-layered Regulation of SPL15 and Cooperation with SOC1 Integrate Endogenous Flowering Pathways at the Arabidopsis Shoot Meristem. *Dev Cell* **37**, 254-266, doi:10.1016/j.devcel.2016.04.001 (2016).
21 Schmid, M. *et al.* Dissection of floral induction pathways using global expression analysis. *Development* **130**, 6001-6012, doi:10.1242/dev.00842 (2003).
22 Daum, G., Medzihradszky, A., Suzaki, T. & Lohmann, J. U. A mechanistic framework for noncell autonomous stem cell induction in Arabidopsis. *Proc Natl Acad Sci U S A* **111**, 14619-14624, doi:10.1073/pnas.1406446111 (2014).

382 23 Fernie, A. R. *et al.* Synchronization of developmental, molecular and metabolic
383 aspects of source-sink interactions. *Nat Plants* **6**, 55-66, doi:10.1038/s41477-020-
384 0590-x (2020).
385 24 Wisman, E., Cardon, G. H., Fransz, P. & Saedler, H. The behaviour of the autonomous
386 maize transposable element En/Spm in Arabidopsis thaliana allows efficient
387 mutagenesis. *Plant Mol Biol* **37**, 989-999, doi:10.1023/a:1006082009151 (1998).
388 25 Forner, J., Pfeiffer, A., Langenecker, T., Manavella, P. A. & Lohmann, J. U. Germline-
389 transmitted genome editing in Arabidopsis thaliana Using TAL-effector-nucleases.
390 *PLoS One* **10**, e0121056, doi:10.1371/journal.pone.0121056 (2015).
391 26 Clough, S. J. & Bent, A. F. Floral dip: a simplified method for Agrobacterium-mediated
392 transformation of Arabidopsis thaliana. *Plant J* **16**, 735-743, doi:10.1046/j.1365-
393 313x.1998.00343.x (1998).
394 27 Mathieu, J., Warthmann, N., Kuttner, F. & Schmid, M. Export of FT protein from
395 phloem companion cells is sufficient for floral induction in Arabidopsis. *Curr Biol* **17**,
396 1055-1060, doi:10.1016/j.cub.2007.05.009 (2007).
397 28 Schwab, R. *et al.* Specific effects of microRNAs on the plant transcriptome. *Dev Cell* **8**,
398 517-527, doi:10.1016/j.devcel.2005.01.018 (2005).
399 29 Wang, Z. P. *et al.* Egg cell-specific promoter-controlled CRISPR/Cas9 efficiently
400 generates homozygous mutants for multiple target genes in Arabidopsis in a single
401 generation. *Genome Biol* **16**, 144, doi:10.1186/s13059-015-0715-0 (2015).
402 30 Ruf, S. *et al.* High-efficiency generation of fertile transplastomic Arabidopsis plants.
403 *Nat Plants* **5**, 282-289, doi:10.1038/s41477-019-0359-2 (2019).
404 31 Varkonyi-Gasic, E., Wu, R., Wood, M., Walton, E. F. & Hellens, R. P. Protocol: a highly
405 sensitive RT-PCR method for detection and quantification of microRNAs. *Plant*
406 *Methods* **3**, 12, doi:10.1186/1746-4811-3-12 (2007).
407 32 Czechowski, T., Bari, R. P., Stitt, M., Scheible, W. R. & Udvardi, M. K. Real-time RT-PCR
408 profiling of over 1400 Arabidopsis transcription factors: unprecedented sensitivity
409 reveals novel root- and shoot-specific genes. *Plant J* **38**, 366-379,
410 doi:10.1111/j.1365-313X.2004.02051.x (2004).
411 33 Kaufmann, K. *et al.* Chromatin immunoprecipitation (ChIP) of plant transcription
412 factors followed by sequencing (ChIP-SEQ) or hybridization to whole genome arrays
413 (ChIP-CHIP). *Nat Protoc* **5**, 457-472, doi:10.1038/nprot.2009.244 (2010).
414 34 Wu, F. H. *et al.* Tape-Arabidopsis Sandwich - a simpler Arabidopsis protoplast
415 isolation method. *Plant Methods* **5**, 16, doi:10.1186/1746-4811-5-16 (2009).
416 35 Yoo, S. D., Cho, Y. H. & Sheen, J. Arabidopsis mesophyll protoplasts: a versatile cell
417 system for transient gene expression analysis. *Nat Protoc* **2**, 1565-1572,
418 doi:10.1038/nprot.2007.199 (2007).
419 36 Schindelin, J. *et al.* Fiji: an open-source platform for biological-image analysis. *Nat*
420 *Methods* **9**, 676-682, doi:10.1038/nmeth.2019 (2012).
421

422 **Acknowledgments**

423 The authors wish to thank all members of the Wahl group for fruitful discussions, T. Seibert, M.
424 Schmid and P. Wigge for critical reading of the manuscript, D. Walter for input on statistical
425 analyses, K. Kontbay, M. Liang and J. Van Dingenen for their support with the *spl*
426 CRISPR/*Cas9* deletion lines, M. Molochko for sharing the *35Somega:LUC-NOS* plasmid, J.
427 Forner for providing the *pJF1031* and *pJF1033* plasmids.

428 **Funding**: Work in the Wahl group was supported by the BMBF (SolaMI, 031B0191), the DFG
429 (SPP1530: WA3639/1-2, 2-1), and the Max Planck Society.

430 **Authors contribution**

431 VW conceived and designed the experiments and prepared the figures with contributions from
432 MML. VW and MML analyzed the data and wrote the manuscript. MML, KF, AK, and VW
433 performed all essential experiments, i.e. VW generated most of the lines used, except for
434 *ML1:amiRTPPJ* (KF), the *spl* CRISPR/*Cas9* deletion lines (MML), and all crosses thereof
435 (MML). MML performed all transactivation assays, ChIP-PCRs, EMSAs and qPCR analyses.
436 MML, AK, KF, CA, and VW analyzed SAM sizes and scored flowering time. RNA *in situ*
437 hybridizations were performed by VW, AK, KF and MML. FK and VW took the confocal
438 images. All authors have read and commented on the text and figures within this manuscript.

439 **Competing interests**

440 Authors declare no competing interests.

441 **Additional Information**

442 Supplementary Information: Figures S1-S22, Tables S1-S7, References (1-3).

443

Figures captions

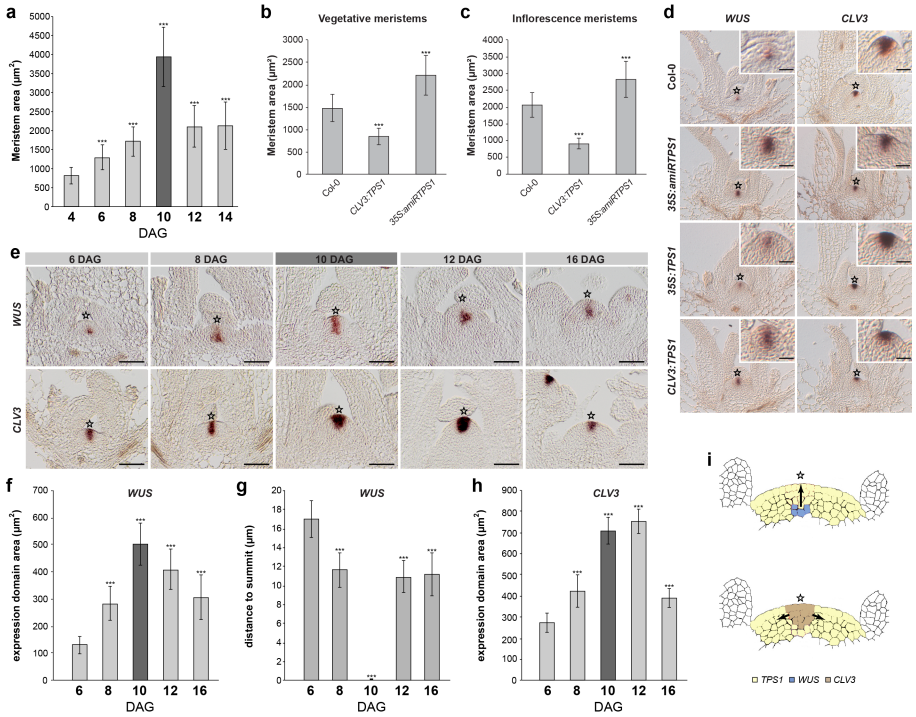

Fig. 1. The T6P pathway impacts SAM size during development. (**a**) SAM area throughout development. (**b**) Vegetative and (**c**) inflorescence SAM size of *CLV3:TPS1* and *35S:amiRTPS1* lines. (**d**) *WUS* and *CLV3* expression by RNA *in situ* hybridisation on longitudinal sections through Col-0, *35S:amiRTPS1, 35S:TPS1* and *CLV3:TPS1* SAMs of LD-grown plants 8 days after germination. (**e**) *WUS* and *CLV3* expression by RNA *in situ* hybridisation in vegetative (6 and 8 DAG), transition (10 DAG, dark grey) and inflorescence SAMs (12 and 16 DAG) of LD-grown Col-0 plants. (**f**) *WUS* expression domain sizes, (**g**) *WUS* expression domain distance to SAM summit, and (**h**) *CLV3* expression domain area, in vegetative, transition (dark grey) and inflorescence SAMs of LD-grown wild-type plants. (**i**) Schematic picture of *WUS, CLV3* and *TPS1* expression dynamics with arrows indicating direction of increasing expression domain at transition. Error bars denote s.d.; significance was calculated based on one-way Annova and a Student's *t*-test, ***P<0.001. ☆ indicates SAM summit. Scale bars 25µm.

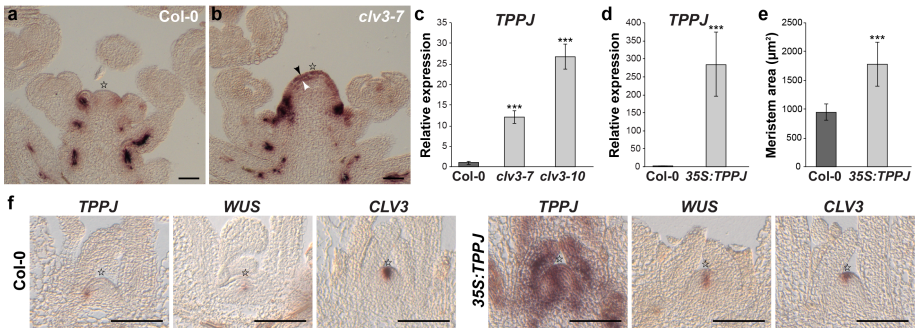

Fig. 2. *WUS* and *CLV3* expression in response to changes of *TPPJ* in the SAM. (**a**, **b**) *TPPJ* expression by RNA *in situ* hybridisation on longitudinal sections through inflorescence SAMs of Col-0 (**a**), and *clv3-7* (**b**), and by qRT-PCR in apices collected from *clv3-7*, *clv3-10* (**c**), and *35S:TPPJ* (**d**) plants. (**e, f**) SAM size of plants overexpressing *TPPJ* (**e**), expression of *TPPJ*, *WUS*, *CLV3* by RNA *in situ* hybridization (**f**). Error bars denote s.d.; significance calculated by one-way Anova and Student's *t*-test, ***P<0.001. ☆ indicates SAM summit. Scale bars are 50µm.

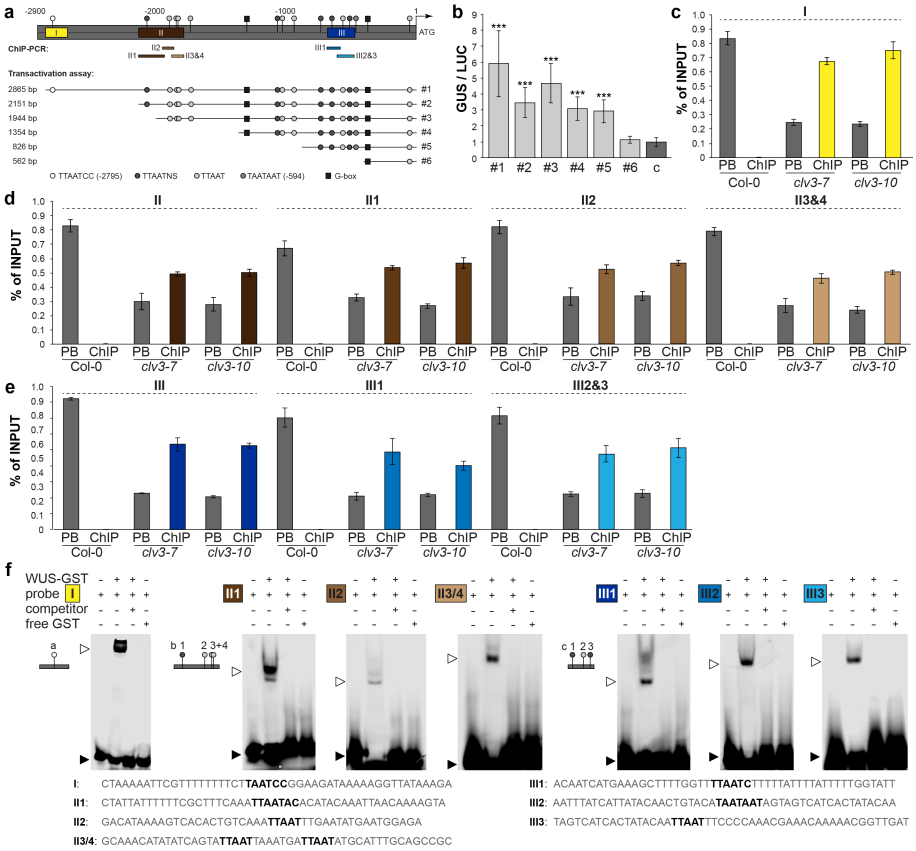

466

467 **Fig. 3. WUS directly regulates *TPPJ* in the SAM.** (**a**) Overview of *TPPJ* 5' regulatory region
468 with putative WUS binding sites (●, ■), position of ChIP-PCR amplicons corresponding to the
469 results shown in (c-e). Boxes marked with I, II, and III indicate 5' TPPJ regions with in total
470 seven core WUS binding sites – **I**: -2795 – -2789 bp, **II**: -2073 – -1830 bp, and **III**: -652 – -564
471 bp. Sequence location and lengths used in (b) indicated with #1-6. (**b**) Protoplast transactivation
472 assay showing activation of the GUS reporter when coupled to the regions indicated in (a),
473 relative to LUC activity. c indicates untransformed control. (**c-e**) Enrichment of (**c**) region I, (**d**)
474 region II, and (**e**) region III as indicated in (a) measured by ChIP-PCR relative to the input. PB –
475 post binding fraction. (**f**) EMSA for WUS binding to the indicated regions (**a**, I-III). Error bars
476 denote s.d.; significance based on one way Anova and Student's *t*-test, ***P<0.001. Scale bars
477 are 50μm.

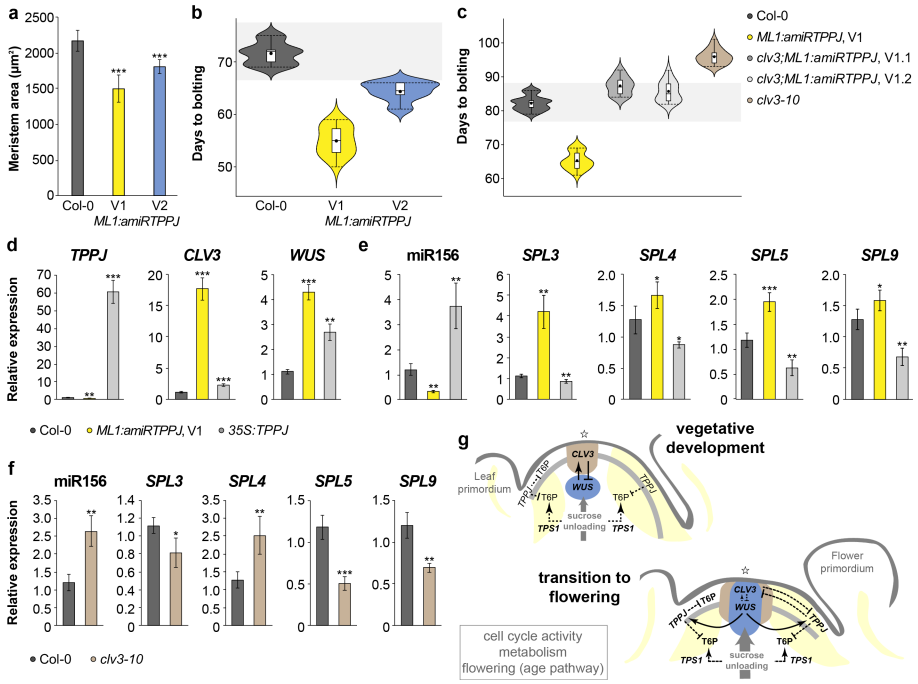

Fig. 4. The role of TPPJ in the outer SAM layer. (**a**) Meristem area of Col-0, *ML1:amiRTPPJ* V1 and V2, (**b-c**) Flowering time of *ML1:amiRTPPJ* (**B**) and *clv3-10;ML1:amiRTPPJ* (**C**) shown as days to bolting (**a**, **c**) relative to the wild type. V1 and V2 indicate two independent versions of artificial microRNAs designed to target *TPPJ* transcript. (**D**, **E**) Relative expression of *SPL* genes, mature miR156 (**d**), and *TPPJ, CLV3*, and *WUS* (**E**) in SD-grown *ML1:amiRTPPJ* and *35S:TPPJ* at 40 days after germination. (**f**) Relative expression of mature miR156 and *SPL* genes in SD-grown *clv3-10* at 40 days after germination. (**g**) Schematic model of vegetative and transition SAM circuits. Error bars denote s.d.; significance calculated based on one way Anova and Student's *t* test; **P*<0.05, ***P*<0.01, ****P*<0.001. ☆ indicates SAM summit.